Strengthening of convective mass fluxes despite weakening of the mean circulation in super-parameterized warming simulations

A. M. Jenney[1], D. A. Randall[1], M. D. Branson[1]

[1]Department of Atmospheric Science, Colorado State University, Fort Collins, CO, USA

Key Points:

- Convective mass fluxes can strengthen despite the weakening of the mean circulation predicted by the weak temperature gradient approximation
- This strengthening of the convective mass flux is made possible by changes in stratiform latent heating and environmental vertical motion
- The warming-induced changes in the convective mass flux depend strongly on the column relative humidity

Corresponding author: Andrea Jenney, `Andrea.Jenney@colostate.edu`

Abstract

Previous work has established that warming is associated with an increase in dry static stability, a weakening of the tropical circulation, and a decrease in the lower-tropospheric convective mass flux. Using both idealized and realistic global warming simulations with super-parameterized convection, we find that the weakening of the tropical circulation can occur at the same time as a *strengthening* of the middle- and upper-tropospheric convective mass flux. Our analysis shows that this strengthening results from changes in the stratiform heating and "environmental" vertical motion that occur in the spaces between the convective clouds.

Plain Language Summary

The circulation of the atmosphere is expected to weaken in a future warmer climate. Despite an expected increase in precipitation, it is thought that near the surface the average strength of stormy updrafts (as measured by the average speed of the updrafts multiplied by the area of the updrafts) will also decrease. We use simulations with realistic representations of storms to test these ideas. Our results show that while the circulation does weaken, the stormy updrafts can actually strengthen aloft. This is made possible by changes in the clouds and vertical motion that occur between the storms.

1 Introduction

The mean tropical circulation is strongly coupled to convection. Mean rising motion occurs over relatively warm and moist regions, in association with active deep cumulus convection. This upward motion is balanced by slow, radiatively driven subsidence that occurs in drier regions, where cumulus convection is suppressed.

For reasons discussed below, both the tropical mean circulation and convective mass flux are expected to weaken in a future, warmer climate (Betts & Ridgway, 1989; Chou & Chen, 2010; Knutson & Manabe, 1995; Held & Soden, 2006; Schneider et al., 2010; Seager et al., 2010; Vecchi & Soden, 2007). The mean circulation is the net vertical mass flux over an area large enough to contain multiple convective updrafts, and is the sum of the convective mass flux of updrafts and downdrafts and the vertical mass flux of the non-convecting environment.

Betts and Ridgway (1989) were the first to suggest a weakening of the tropical mean circulation with warming. Using a simple model of the tropical boundary layer, they found that the subsidence required for thermodynamic equilibrium weakened as sea surface temperatures warmed. Their conclusions were supported by the results of Knutson and Manabe (1995), who found that a global circulation model (GCM) simulated a weakening of the circulation with warming.

This result can be understood in terms of the area-averaged dry static energy budget:

$$\frac{\partial \overline{s}}{\partial t} = -\overline{\mathbf{v}_h} \cdot \nabla \overline{s} - \overline{\omega}\frac{\partial \overline{s}}{\partial p} + \overline{Q_R} + \overline{Q_c}. \quad (1)$$

Here s is dry static energy, $\mathbf{v}_h$ is the horizontal wind vector, ω is the vertical pressure velocity, Q_R is the radiative heating rate, Q_c is the non-radiative heating rate due to cloud processes and turbulence, and an overbar represents an average over an area comparable to that of a GCM's grid cell. In a dry-statically stable atmosphere, $\partial s/\partial p < 0$. In the tropics and for time scales longer than a few hours or a day at most, equation (1) can be approximated by the "weak temperature gradient" (WTG) balance (Charney, 1963; Sobel & Bretherton, 2000; Sobel et al., 2001):

$$\overline{\omega}\frac{\partial \overline{s}}{\partial p} = \overline{Q_R} + \overline{Q_c}. \quad (2)$$

In the absence of non-radiative heating (i.e., for $\overline{Q_c} = 0$), (2) reduces to a balance between radiative cooling ($\overline{Q_R} < 0$) and the warming due to downward advection of dry static energy (i.e., $\overline{\omega} > 0$). Many studies have shown that in a warming climate the tropical static stability increases to match the more stable moist adiabat associated with warmer surface temperatures. The fractional change in the static stability is larger than the fractional change in the radiative cooling rate, so that (2) implies a weakening of the subsidence. Mass conservation then ensures that the mean upward mass flux in convectively active regions also weakens.

Held and Soden (2006) proposed that the globally averaged convective mass flux will also decrease with warming. This is the mass flux associated with convective updrafts (and downdrafts). Their argument is based on consideration of the globally averaged moisture budget in the form

$$\overline{\overline{P}} = \overline{\overline{M_B}}\,\overline{\overline{q_B}}. \tag{3}$$

Here a double overbar denotes a global average, P is the surface precipitation rate, M_B is the convective mass flux at the top of the boundary layer associated with precipitating convection, and q_B is the water vapor mixing ratio in the boundary layer. The globally averaged latent heat release associated with precipitation is mainly balanced by changes in atmospheric radiative cooling (e.g., Riehl & Malkus, 1958). Allen and Ingram (2002) argued that as the climate warms, the fractional increase in $\overline{\overline{P}}$ will be much smaller than the fractional change of $\overline{\overline{q_B}}$, which increases following Clausius-Clapeyron scaling. Based on this idea, Held and Soden (2006) concluded from (3) that $\overline{\overline{M_B}}$ must decrease with warming. Vecchi and Soden (2007) provided support for this conclusion, based on an analysis of results from a suite of GCMs.

In summary, energy balance suggests that the mean circulation will weaken with warming, and moisture balance suggests that the near-surface convective mass flux will weaken with warming. Caution is needed, however. There are important differences between the mean vertical motion and the convective mass flux (Arakawa & Schubert, 1974; Betts, 1998), because the former includes partially cancelling contributions from much stronger local convective updrafts and downdrafts, as well as vertical motions in the broad environment between the convective drafts. For example, Schneider et al. (2010) estimated that the rate at which mass ascends in convective updrafts may be up to 5 times larger than the mean upward motion, simply because of compensating downward motions in the same region.

The current paradigm of warming-induced weakening of both the tropical convective mass flux and the tropical mean circulation deserves further study, in part because a weakening of the tropical circulation and/or convective mass flux may contribute to a weakening of teleconnections to middle latitudes (Bui & Maloney, 2018, 2019; Wolding et al., 2017). We show in this paper that the free-tropospheric convective mass flux can intensify even as the mean tropical circulation weakens. We offer an explanation of this result based on an energy-balance analysis.

2 Methods

Simulations of the future climate are sensitive to convective parameterizations (e.g., Maher et al., 2018). This problem can be avoided by using convection-resolving models (CRMs; e.g., Stevens et al., 2019). Unfortunately, the high computational cost of such models limits their use in global climate change simulations, for now. Superparameterization offers an intermediate option, in which conventional parameterizations of cloud and boundary-layer processes are replaced with a CRM embedded within each GCM grid cell (Grabowski, 2001; Khairoutdinov & Randall, 2001; Randall et al., 2003). Superparameterization has been shown to enable more realistic simulations of a number of convectively coupled global processes (reviewed by Randall et al., 2016). Key for the present study is that super-parameterization makes it possible to directly diagnose changes in the convective mass flux, which is explicitly simulated by the CRM, rather than parameterized.

We have used superparameterized versions of the Community Atmosphere Model (CAM) and Community Earth System Model (CESM) to explore changes to the convective mass flux and circulation with warming. We will show results from both idealized and realistic simulations to assess the robustness and limitations of the theoretical ideas outlined in Section 1, in connection with equations (2) and (3). The simulations are described further in the remainder of this section. We present our results in section 3, and conclusions in section 4.

2.1 Radiative-Convective Equilibrium

We used a super-parameterized version of CAM4, with the finite-volume dynamical core and a $0.9° \times 1.25°$ horizontal grid. Each GCM grid column hosts an embedded two-dimensional CRM. The embedded CRMs have a horizontal grid spacing of 4 km and use 32 columns. They share the bottom 24 of CAM4's 26 layers. We use a single-moment microphysics scheme. For more details see Khairoutdinov et al. (2005).

Following the experimental design of the radiative-convective equilibrium model intercomparison project (RCEMIP; Wing et al., 2018), we simulated radiative-convective equilibrium using uniform solar insolation and uniform sea surface temperatures (SSTs) on a non-rotating planet. Using SSTs of 295 K, 300 K, and 305 K, we ran the model for three simulated years. Our results are based on analysis of monthly mean output for year

3, and daily mean output from a 30-day extension at the end of year 3. Data were saved on the native CAM4 0.9° × 1.25° horizontal grid, and for 26 hybrid-sigma model levels. We linearly interpolated to 26 pressure levels for analysis.

2.2 Earth simulations with 4×CO_2 warming

We have also analyzed simulations with a more realistic version of the model. We will refer to these as the "earth" simulations. They are based on SP-CESM1, which is a coupled atmosphere-ocean-land-sea ice earth system model with super-parameterization in the CAM5 atmosphere model, again with the finite-volume dynamical core. We compare a simulation with pre-industrial (PI) concentrations of atmospheric CO_2 (PI-control) to a simulation with 4 times the CO_2 of the PI-control simulation (4×CO_2). Both simulations are ten-year SP-CESM1 branches from much longer CESM1 simulations. A more detailed description of the earth simulations is given by Burt (2016).

Unless otherwise stated, we present results for the last 5 years of each simulation, based on monthly mean model output. Data were saved onto the CAM5 1.9°×2.5° horizontal grid, and onto 30 hybrid-sigma model levels in the vertical. We linearly interpolated the vertical grid to 30 constant pressure levels. For the earth simulations, we limit our analysis to the tropics between 20°S-20°N, including both ocean and land points.

We note that the earth simulation with 4×CO_2 is influenced by the direct radiative forcing from the increased concentration of CO_2, which by itself tends to weaken the large-scale circulation relative to the pre-industrial simulation (Merlis, 2015). This is in contrast to the warming of the RCE simulations, which is due only to the specified increase in the globally uniform SST.

2.3 Diagnostics

For both the RCE and earth simulations, we make use of diagnostic variables computed by the CRM and saved on the GCM grid. These are the non-radiative temperature tendency due to the embedded CRM (model variable name "SPDT"), and the updraft and downdraft convective mass fluxes. Four categories of convective mass fluxes are calculated for each layer of the CRM: cloudy updrafts ("SPMCUP"), unsaturated updrafts ("SPMCUUP"), cloudy downdrafts ("SPMCDN"), and unsaturated downdrafts ("SPMCUDN"). The convective mass fluxes receive contributions from only those CRM

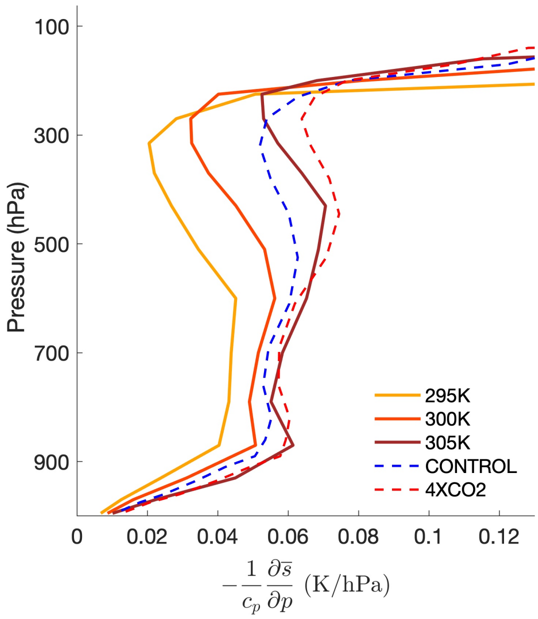

Figure 1. Mean static stability profiles for RCE (solid) and Earth (dashed) simulations.

grid cells for which the sum of the vertical velocities at the layer top and bottom is greater than 4 m s^{-1} (updrafts) or less than -4 m s^{-1} (downdrafts). "Cloudy" mass fluxes are saved when the sum of the cloud water and cloud ice mixing ratios exceeds 1 g kg^{-1}. Otherwise the mass flux is categorized as unsaturated. We refer to the sum of the four convective updraft and downdraft mass fluxes as the net convective mass flux.

3 Results

3.1 Analysis of the RCE simulations

The global-mean precipitation rate increases from 2.6 mm day^{-1} in the 295 K RCE simulation to 3.2 mm day^{-1} (a 3.9 % K^{-1} increase) and 3.7 mm day^{-1} (3.2 % K^{-1}) in the 300 K and 305 simulations, respectively. As expected for a boundary layer that is warming but maintaining roughly constant relative humidity, the simulated increase in low-level water vapor mixing ratio is between 6.5-7 % K^{-1}.

The solid lines in Figure 1 show the domain-mean static stability profiles for these simulations. The static stability increases with warming, particularly at upper-levels, as expected for a tropical lapse rate adjusting to a warmer moist adiabat.

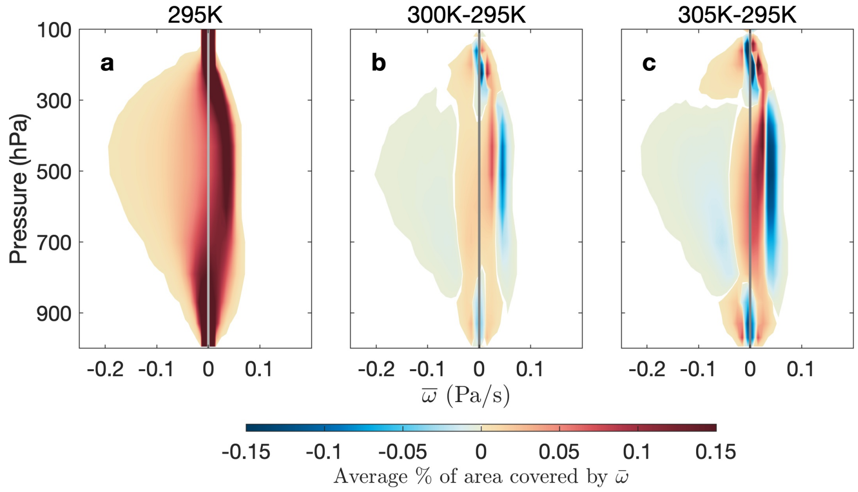

Figure 2. Probability distributions of $\overline{\omega}$ in the RCE simulations, based on monthly mean data, in percent of global area covered. a, the distribution for the 295 K simulation. b, the difference between the 300 K and 295 K simulations. c, the difference between the 305K and 295K simulations.

As mentioned earlier, a weakening of the mean circulation is an expected response to warming. Figure 2 shows the vertically resolved distribution of grid-scale vertical velocities ($\overline{\omega}$) for the 295 K simulation, and the differences between the warmer simulations and the 295 K simulation. The shading represents the average monthly mean percent of global area covered in a $\overline{\omega}$ bin. In panel a, darker colors indicate that a large percentage of the globe has a value of $\overline{\omega}$ in that bin. In panels b and c, the shading represents the same quantity, except that it now shows *changes* between two simulations. Panel a shows that the mean circulation includes broad regions of weak sinking motion and narrow regions of more vigorous rising motion. Panels b and c show the expected weakening of the monthly mean $\overline{\omega}$. This is seen as a narrowing of the $\overline{\omega}$ distribution, which means that strong grid-scale rising and sinking motions become less common, while weak values become more common. The exception is above about 300 hPa, where an increase in stronger vertical motion at the expense of weaker values reflects the deepening of the convective layer (and the troposphere) with warming. We find the same pattern of grid-scale circulation weakening in distributions of the daily-mean $\overline{\omega}$ (not shown).

We will use the pressure velocity, ω, to quantify the various vertical mass fluxes. For a GCM grid cell, the mass flux of the mean circulation, $\overline{\omega}$, can be written as the sum

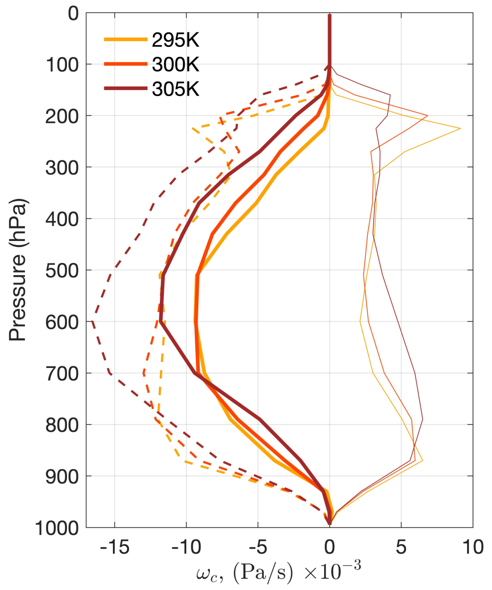

Figure 3. Global mean profiles of ω_c (thick solid) for the RCE simulations, the global mean updraft (dashed) and downdraft ω_c (thin solid).

of the net convective mass flux ω_c and the "environmental" mass flux $\tilde{\omega}$ (Arakawa & Schubert, 1974):

$$\overline{\omega} = \omega_c + \tilde{\omega}. \tag{4}$$

Area weighting is included in the definitions of ω_c and $\tilde{\omega}$. The environmental mass flux is associated with weak vertical motions in the broad regions between the convective updrafts and downdrafts. It is typically but not always downward. Eq. (4) shows that when convection is not active the mean mass flux is equal to the environmental mass flux.

Figure 3 shows global-mean profiles of the convective mass fluxes for the 295 K, 300 K, and 305 K RCE simulations. Consistent with previous work suggesting a weakening of the low-level convective mass flux with warming (Held & Soden, 2006; Emanuel, 2019), we find a weakening of both the net ω_c and the updraft ω_c between the 295 K and warmer simulations below about 700 hPa (800 hPa for the updraft ω_c). Between about 900 and 800 hPa, this weakening of then net mass flux is mainly due to a weakening of the updrafts. Above 800 hPa, the updrafts strengthen between the 295 K and warmer simulations. The weakening of the net ω_c between 800 and 700 hPa is due to a strength-

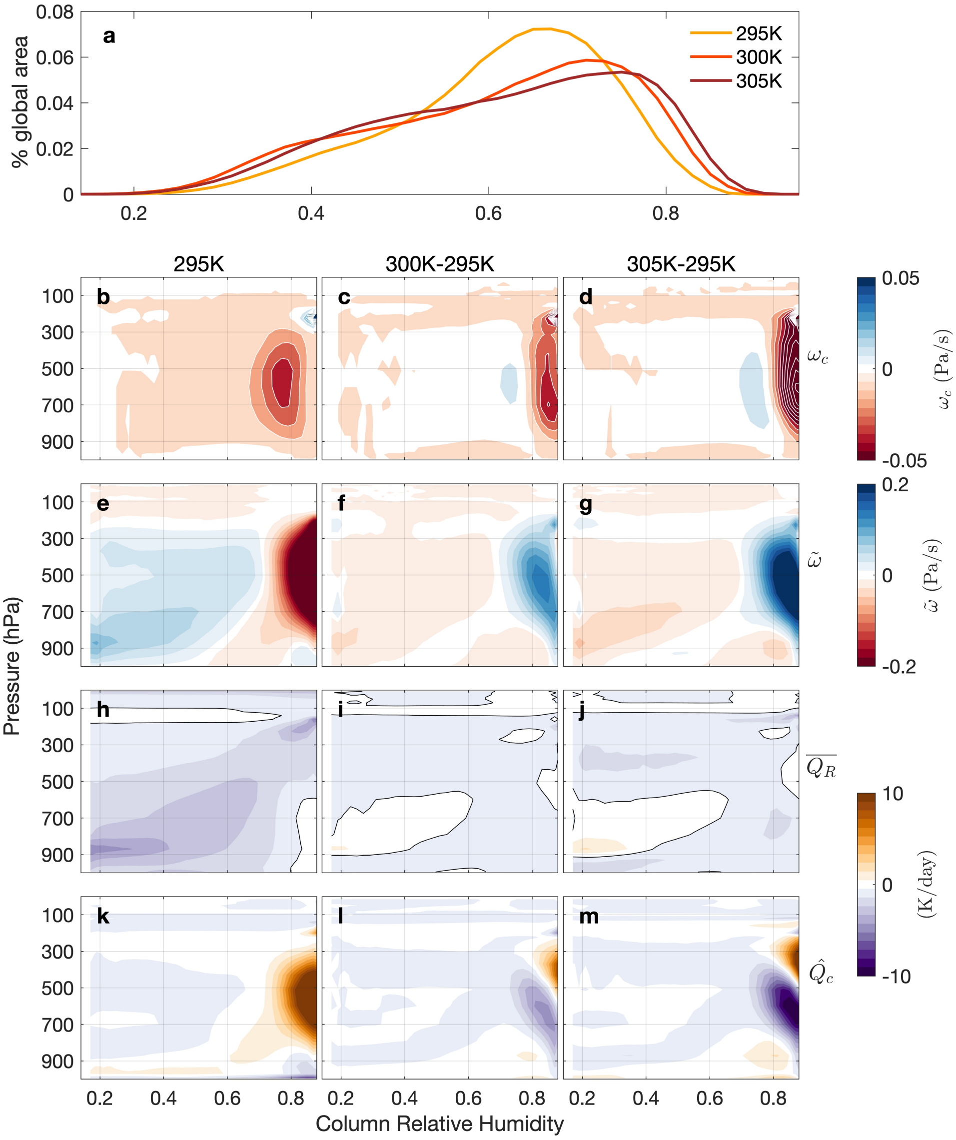

Figure 4. a, Probability distributions of daily mean column relative humidity values for bins 0.02 wide, in average daily percent of global area covered. b-m, daily mean convective mass flux, environmental mass flux, stratiform heating, and radiative heating binned by column relative humidity for the 295K simulation, and the difference between the 295 K and warmer simulations. Solid black contours in h-j reference the zero line.

ening of the downdrafts at these levels. Below about 900 hPa, the updraft and downdraft convective mass fluxes are insensitive to the surface temperature.

Figure 3 shows that despite the weakening of the mean circulation throughout the troposphere, there is a *strengthening* of the global mean ω_c above 700 hPa. Some insight into this result can be gained from Figs. 4b-d, which show ω_c binned by column relative humidity for the 295 K simulation and the differences between the warmer simulations and the 295 K simulation. Column relative humidity is the column precipitable water divided by the column precipitable water for a saturated column with the same temperature profile. The figures show that the invigoration of convective mass fluxes is occurring in columns with column relative humidities greater than 80%. This invigoration is accompanied by a broadening of the column relative humidity distribution to include more extreme values (Figure 4a) which may be indicative of more organized convection (e.g., Chou & Neelin, 2004). These results show that there is a strengthening of intense convection in the warmer climate.

Figures 4c and d also show that the weakening of the low-level convective mass fluxes seen in the global mean profiles (Figure 3) is not occurring in the same columns for which there is an invigoration of upper-level convective mass fluxes. The strengthening of the mean free-tropospheric ω_c with warming shown in Figure 3 occurs almost entirely in very humid columns. In these very humid grid cells, ω_c strengthens throughout the troposphere. The weakening of low-level (below 800 hPa) ω_c in the global mean profiles occurs in relatively dry columns.

Given the relationship between ω_c and $\overline{\omega}$, as expressed in equation (4), a strengthening of ω_c can occur despite a weakening of $\overline{\omega}$ if there is a change in $\tilde{\omega}$ such that the sum $\omega_c+\tilde{\omega}$ decreases with warming. Figure 4e-g shows $\tilde{\omega}$ binned by column relative humidity for the 295 K simulation and the differences between the warmer simulations and the 295 K simulation. For columns with column relative humidities less than about 70%, which include most of the domain in the 295 K simulation, $\tilde{\omega}$ is downwards, while the convective mass flux is upwards. In contrast, $\tilde{\omega}$ is strongly upwards for the most humid columns. Figure 4 shows that the strengthening of the convective mass flux is accompanied by a weakening of the upward environmental mass flux.

Next, we will show how a simultaneous strengthening of convective mass fluxes and weakening of the mean circulation is consistent with the WTG framework. For averages over areas (such as a GCM grid cell) large enough so that the fractional area occupied by convective updrafts is $\ll 1$ (Arakawa & Schubert, 1974), $\overline{Q_c}$ may be written as

$$\overline{Q_c} = \omega_c \frac{\partial \overline{s}}{\partial p} + L\tilde{C} + \overline{D}(s_c - \overline{s}) + \overline{Q_{turb}}, \tag{5}$$

where $\omega_c \partial \overline{s}/\partial p$ is the warming due to the net convective mass flux, L is the latent heat of condensation, $\tilde{C}$ is the environmental condensation rate, $\overline{D}$ is the detrainment mass flux, and $\overline{Q_{turb}}$ is the dry static energy transport due to turbulence. Equations (4) and (5) allow us to rewrite (2) as

$$\tilde{\omega} \frac{\partial \overline{s}}{\partial p} = \overline{Q_R} + \hat{Q}_c, \tag{6}$$

where we define

$$\hat{Q}_c \equiv L\tilde{C} + \overline{D}(s_c - \overline{s}) + \overline{Q_{turb}} \tag{7}$$

as the (non-radiative) cloud and turbulent heating apart from (i.e., not including) the contribution from $\omega_c \frac{\partial \overline{s}}{\partial p}$. Contributions to $\hat{Q}_c$ come from environmental (non-convective) condensation $L\tilde{C}$, convective detrainment of dry static energy $D(s_c - \overline{s})$, and turbulent transport of dry static energy, but for simplicity we refer to $\hat{Q}_c$ as the "stratiform heating." Houze (1977) emphasized that condensation in stratiform anvil clouds is a major component of the heating in tropical convective systems. We expect $L\tilde{C} > 0$ where there is environmental rising motion in stratiform anvil clouds, and $L\tilde{C} < 0$ where rain is evaporating (or snow is melting) as it falls through an unsaturated portion of the environment. Using equations (5) and (7), we can compute $\hat{Q}_c$ for each grid cell in our simulations as $\hat{Q}_c = \overline{Q_c} - \omega_c(\partial \overline{s}/\partial p)$.

Writing WTG balance in terms of $\tilde{\omega}$, as in equation (6), allows us to diagnose the relevant terms in the heating balance important for the environmental mass flux of a large area, regardless of whether or not the area contains convection (Arakawa & Schubert, 1974; Chikira, 2014). For grid cells containing active convection, equation (6) says that the dry static energy advection by the environmental mass flux, $\tilde{\omega}(\partial \overline{s}/\partial p) = (\overline{\omega} - \omega_c)(\partial \overline{s}/\partial p)$, balances the combination of stratiform heating and radiative cooling. For grid cells that don't contain active convection, $\omega_c = 0$, $\tilde{\omega} = \overline{\omega}$, $\hat{Q}_c$ is typically negligible, and equation (6) reduces to a balance between radiative cooling and advection of dry static energy by the mean vertical motion.

As mentioned previously, a weakening of $\overline{\omega}$ is possible despite a strengthening of ω_c if there is a compensating change in $\tilde{\omega}$. The two possibilities are: 1) a strengthening of $\tilde{\omega}$ where $\tilde{\omega}$ is downward (which occurs in drier grid columns), and 2) a weakening of $\tilde{\omega}$ where $\tilde{\omega}$ is upwards (which occurs in the wettest grid columns). In both of these scenarios, the change in $\tilde{\omega}$ is positive.

We can estimate the fractional change in $\tilde{\omega}$ in equation (6) as the difference between the fractional changes in $\overline{Q_R} + \hat{Q}_c$ and $\partial\overline{s}/\partial p$:

$$\frac{\Delta\tilde{\omega}}{\tilde{\omega}} \approx \frac{\Delta(\overline{Q_R} + \hat{Q}_c)}{\overline{Q_R} + \hat{Q}_c} - \frac{\Delta\frac{\partial\overline{s}}{\partial p}}{\frac{\partial\overline{s}}{\partial p}}. \tag{8}$$

We now identify the conditions required for $\Delta\tilde{\omega} > 0$ by considering four cases, two of which can be discarded because they do not obey equation (6).

Cases 1 and 2 ($\tilde{\omega} > 0$): Where the environmental mass flux is downward, the left-hand side of equation (8) must be positive. It follows that the combination of the two terms on the right-hand side must also be positive. This can happen if the fractional change in $\overline{Q_R}+\hat{Q}_c$ is greater than the fractional change in dry static stability. We can distinguish two cases, one where $\overline{Q_R} + \hat{Q}_c > 0$ (case 1) and the other with $\overline{Q_R} + \hat{Q}_c < 0$ (case 2). Case 1 can be discarded because it does not obey (6). In Case 2, the only way for the fractional change in $\overline{Q_R}+\hat{Q}_c$ to be greater than the fractional change in dry static stability is if $\overline{Q_R}+\hat{Q}_c < 0$. Panels h-j of Figure 4 show $\overline{Q_R}$ conditioned by column relative humidity for the 295 K simulation and the difference in $\overline{Q_R}$ between the 295 K and warmer simulations. The black lines reference the zero contour. Over most of the region where $\tilde{\omega} > 0$, $\Delta\overline{Q_R} > 0$, i.e., we have either more radiative warming or less radiative cooling. The only way for $\Delta\tilde{\omega}$ to be positive in these regions is for $\Delta\hat{Q}_c$ to shift towards negative values by more than the increase in $\overline{Q_R}$, for example due to a strengthening of the evaporation of falling rain. This seems unlikely.

Cases 3 and 4 ($\tilde{\omega} < 0$): Where the environmental mass flux is upward, the left-hand side of equation (8) must be negative. This is possible if the fractional change in $\overline{Q_R}+\hat{Q}_c$ is less than the fractional change in dry static stability. We can distinguish two cases, one in which $\overline{Q_R} + \hat{Q}_c > 0$ (case 3) and the other with $\overline{Q_R} + \hat{Q}_c < 0$ (case 4). Case 4 can be discarded because it does not obey (6). In Case 3, because of increases in dry static stability, $\Delta(\overline{Q_R}+\hat{Q}_c)$ can be zero! It can also be less than zero, but only to the extent that $\overline{Q_R} + \hat{Q}_c$ remains positive.

In summary, we conclude that Case 3, with $\tilde{\omega} < 0$ and $\overline{Q_R}+\hat{Q}_c > 0$, is the most plausible scenario that is consistent with $\Delta\tilde{\omega} > 0$. Figure 4 shows that this is indeed what we find. The largest increases in ω_c (panels c,d) occur where $\tilde{\omega} < 0$ (panel e) and $\overline{Q_R}+\hat{Q}_c > 0$ (panels h,k).

In places where $\tilde{\omega}$ is upwards, and neglecting the small contributions from detrainment and turbulence, we can approximate $\hat{Q}_c$ in terms of the advection of environmental moisture by $\tilde{\omega}$ as,

$$\hat{Q}_c \approx -\tilde{\omega} L \frac{\partial \tilde{q}}{\partial p}, \quad (\tilde{\omega} < 0), \tag{9}$$

where $\tilde{q}$ is the water vapor mixing ratio of the environment. Combining equations (6) and (9), we then can write

$$\tilde{\omega}\frac{\partial \tilde{h}}{\partial p} \approx \overline{Q_R}, \tag{10}$$

where $\tilde{h} = \overline{s} + L\tilde{q}$ is the environmental moist static energy, using the approximation that $\tilde{s} \approx \overline{s}$ (Arakawa & Schubert, 1974). Equation (10) states that over a large area the vertical advection of $\tilde{h}$ by $\tilde{\omega}$ approximately balances the area-mean radiative heating rate. Again, equation (10) applies only where $\tilde{\omega} < 0$.

The bottom row of Figure 4 shows $\hat{Q}_c$ for the 295K simulation and its differences in the warmer simulations. For humid columns, the cooling due to upward $\tilde{\omega}$ is balanced by a net heating, most of which is due to positive values of $\hat{Q}_c$ (Figure 4h). As shown in (9), upward environmental motion in the most humid columns transports water vapor upwards, driving condensation and latent heat release. A weakening of the upward $\tilde{\omega}$ in the very humid columns, due in part to increases in static stability, is self-reinforcing due to a weakening of the heating from environmental condensation. We conclude that increases in static stability reinforce a weakening of $\tilde{\omega}$ where $\tilde{\omega} > 0$.

Figure 4 also shows a modest weakening of negative $\hat{Q}_c$ at very low levels, which could be due to decreases in rain evaporation and increases in precipitation efficiency (e.g., Lutsko & Cronin, 2018).

In summary, we find that in super-parameterized global simulations of radiative-convective equilibrium the free-tropospheric convective mass flux strengthens at the same time that the mean vertical motion weakens. The strengthening of the convective mass flux occurs where column relative humidities exceed 80% and the environmental mass flux is upward. For these humid columns, increases in dry static stability, which favor a weakening of the mean circulation, may actually favor a strengthening of the convective mass flux through a self-reinforcing weakening of the environmental mass flux involving stratiform heating.

3.2 Analysis of the earth simulations

The RCE aquaplanet simulations are extreme idealizations of the tropics. We now analyze the results obtained with the "earth" configuration of the model, limiting our attention to the tropical zone between 20°S-20°N, including both ocean and land points. Do the earth simulations behave like the RCE simulations?

The global mean surface temperature increases from 289 K to 293 K between the PI-control and $4\times CO_2$ simulations. The global mean surface precipitation rate increases from 2.9 mm day^{-1} to 3.1 mm day^{-1}, which is about 1.2 % K^{-1}. As in the RCE simulations, the global mean low-level water vapor mixing ratio increases more rapidly, at about 5.5-6 % K^{-1}. The dashed lines in Figure 1 show the tropical mean static stability profiles for the earth simulations. As in the RCE simulations, the static stability increases with warming, especially in the upper troposphere.

Figure 5 shows the change in the distribution of monthly mean $\overline{\omega}$ for all tropical columns between 20°S and 20°S, including land points. The weakening of grid-scale vertical motions seen in the RCE simulations is also apparent in the earth simulations. As expected, strong mean rising and sinking motions become less frequent. The same pattern of weakening is also seen in daily means of $\overline{\omega}$ (not shown).

Figure 6a shows changes to the tropical mean ω_c. In contrast with the RCE results, there is no change in the peak tropical mean value of ω_c, and the low-level convective

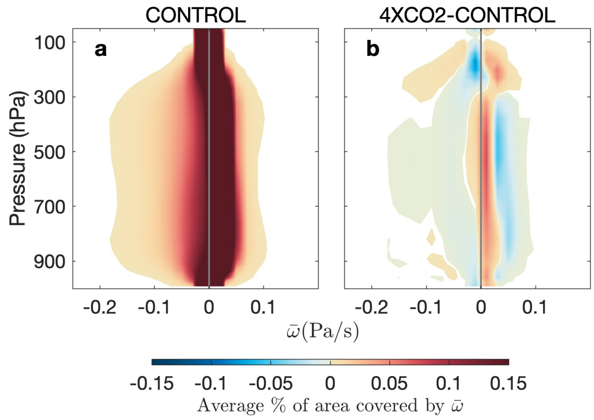

Figure 5. a, Distribution of monthly mean $\overline{\omega}$, in average monthly mean percent of tropical area covered, in the PI-control simulation and b, difference from the 4×CO_2 simulation

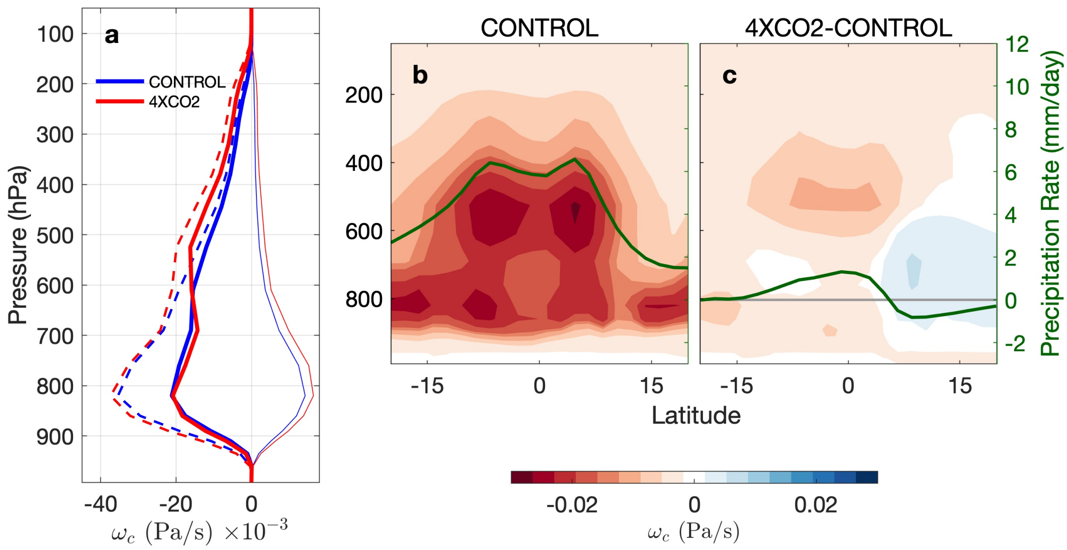

Figure 6. a, Tropical mean (20°S-20°N), net ω_c (thick solid), updraft ω_c (dashed), and downdraft ω_c (thin solid) for the earth simulations. b-c, zonal mean ω_c (contours) and precipitation rate (green curves) for the PI-control simulation (center column) and difference between the 4×CO_2 and PI-control simulations (right column). The zonal means do not include contributions from grid cells where the pressure levels are “underground.”

mass flux does not weaken. The slight increase in ω_c between the PI-control and $4{\times}CO_2$ simulations above 600 hPa appears to be consistent with the deepening of the troposphere with warming. Also shown in Figure 6a are tropical mean profiles of the convective updraft and downdraft mass fluxes. These both strengthen weakly with warming, throughout the column. The tropical mean pattern of change is not representative of individual regions, however. For example, Figure 6b-c show the annual mean zonal mean ω_c and precipitation rate across the tropics for the PI-control simulation and its difference from the $4{\times}CO_2$ simulation. The top-heavy strengthening of ω_c between about 15°S–5°N is consistent with previous work suggesting a preferential increase in upper-tropospheric updraft speeds with warming (Muller et al., 2011; Singh & O'Gorman, 2015). The pattern of near-equatorial convective strengthening and subtropical weakening reflects the narrowing of the intertropical convergence zone with warming (reviewed in Byrne et al., 2018), which is also seen in the change of the zonal mean annual mean precipitation rate (green curves in Figure 6b,c). Figure 6 is for annual mean values of ω_c. The near-zero change in the tropical mean ω_c between 20°S-20°N, the enhanced upper-level strengthening of ω_c over deep convective latitudes, and the narrowing of the deep convective region is also seen in the individual solstice seasons (i.e., means over December-February and over June-August).

Figure 7 shows ω_c, $\tilde{\omega}$, $\overline{Q_R}$, and $\hat{Q}_c$ binned by column relative humidity for the earth simulations. Here, we have used 40 days of daily mean data starting at the beginning of January. As in the RCE simulations, we see an intensification of ω_c only for the most humid columns, in addition to a slight shift of the distribution towards more humid columns. This strengthening is coincident with a weakening of upwards $\tilde{\omega}$ in the most humid columns. We also see a weakening of $\hat{Q}_c$, except at the upper levels, for the most humid columns. Although there is no change in the tropical mean ω_c in the earth simulations, we see the same column relative humidity-conditioned change that appears in the RCE simulations. This indicates that the mechanisms permitting a simultaneous strengthening of ω_c and weakening of the circulation are not sensitive to the experimental design. However, the net change in the tropical mean convective mass flux is sensitive to changes in the spatial distribution of moisture and convection, which is sensitive to the pattern of SST change (Ma & Xie, 2013) and clouds (e.g., Ceppi & Hartmann, 2016; Merlis, 2015; Voigt & Shaw, 2015; Su et al., 2014; Feldl et al., 2014) with warming. Profiles of the tropical mean ω_c subset between 10°S-10°N, instead of the 20°S-20°N shown in Figure 6a, show the same

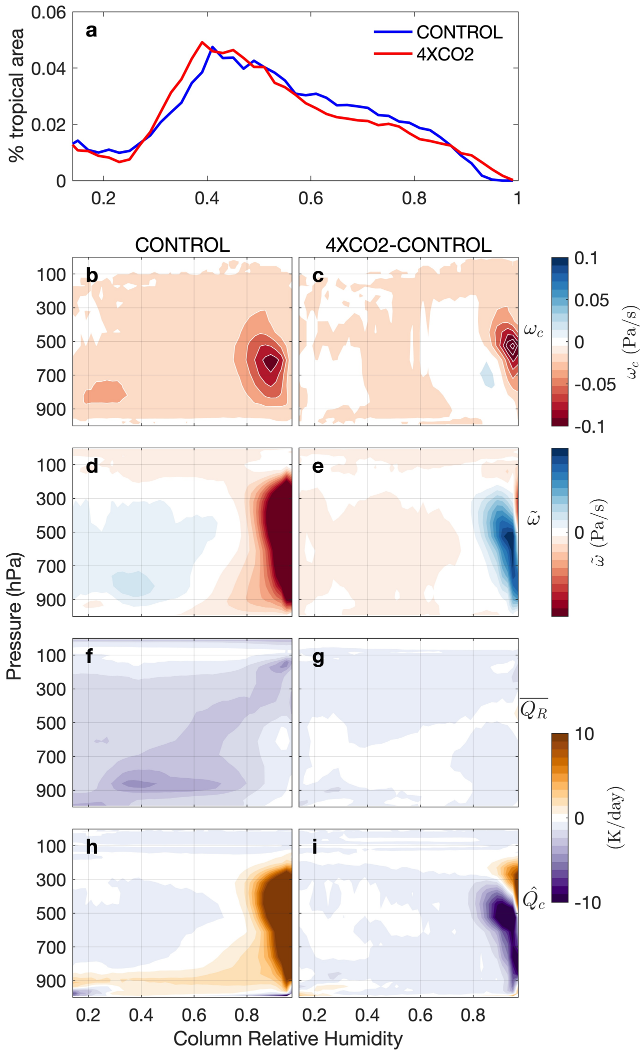

Figure 7. As in Figure 4, but for the tropics (20°S-20°N) in the earth simulations.

strengthening of ω_c observed in the RCE simulations (not shown). The near net zero change in ω_c observed between 20°S-20°N is supported by both a strengthening of free tropospheric ω_c in the deep tropics, and a weakening in the subtropics. Again, this is consistent with the previously mentioned narrowing of the intertropical convergence zone. The tropical mean ω_c strengthens with surface warming in our simulations of global radiative-convective equilibrium, but does not change in our earth simulations, despite a weakening of the mean circulation in both experiments. This shows again that changes in the tropical mean ω_c with warming may not be predicted by changes to the mean circulation.

4 Discussion and Conclusions

The weakening of the tropical circulation can be understood by considering the tropical clear-sky energy balance. The atmosphere is continuously losing energy radiatively, and this energy sink is balanced by adiabatic sinking and warming. For a given radiative cooling rate, the strength of the sinking motion is dictated by the mean tropical static stability profile, which is nearly constant throughout the tropics due to the inability of the tropical atmosphere to support strong pressure gradients. The tropical static stability profile roughly follows a moist adiabat, and will likely become more stable with surface warming in addition to becoming more stable in direct response to increased CO_2 (Merlis, 2015). Increased static stability makes sinking motions over clear-sky regions more efficient, so that for a given amount of radiative cooling less sinking is required to maintain energy balance.

Our results support previous work suggesting a weakening of tropical mean circulations with warming. Consistent with Held and Soden (2006), we find decreases in the convective mass flux near the top of the atmospheric boundary layer in our radiative-convective equilibrium (RCE) simulation. However, we find that the mean convective mass flux strengthens above the boundary layer in the RCE simulations, and does not change in the earth simulations.

When we condition quantities by their column relative humidity, we find that in both our RCE and earth simulations there is a preferential strengthening of convective mass fluxes occurring in very humid columns where environmental mass fluxes, or the vertical motion in the spaces between convective up and downdrafts, are upwards. In these columns, perturbations in dry static stability with warming may enable a strengthening of convective mass fluxes, through a self-reinforcing weakening of the environmental mass flux. Upward environmental mass fluxes in very humid columns warm the environment through stratiform condensation. Increases in dry static stability make it possible for a weaker upward environmental mass flux to balance stratiform heating of the environment. At the same time, a weakening of the environmental mass flux decreases the rate of stratiform heating, which lessens the total diabatic heating which the environmental mass flux balances.

Differences in the change of the convective mass flux between our simulations appear to be related to differences in the pattern of tropical humidity change. In radiative-convective equilibrium we find a shift in the distribution of column relative humidities towards more extreme values. The preferential strengthening of convective mass fluxes in only very humid columns combined with the increase in the number of columns that are very humid is reflected in the increase of the mean tropical convective mass flux. However, in our earth simulations, despite the same humidity-conditioned pattern of convective mass flux change, the narrowing of the intertropical convergence zone results in a net-zero change in the tropical mean convective mass flux. That is, convective mass fluxes strengthen over the deep tropics, but weaken in the subtropics. In summary, our results show that that the tropical mean convective mass flux can change independently of the weakening of the circulation predicted by WTG balance.

Acknowledgments

We thank Prof. Elizabeth Barnes for helpful discussions. Funding support for this project comes from the National Oceanographic and Atmospheric Administration under Grant number NA19OAR4590155 to Colorado State University. The simulations were performed using computational support from the National Center for Atmospheric Research (Cheyenne; doi:10.5065/D6RX99HX). The data used in this study is available from the Mountain Scholar institutional repository managed by Colorado State University. It can be accessed online (`https://hdl.handle.net/10217/199724`).

References

Allen, M. R., & Ingram, W. J. (2002). Constraints on future changes in climate and the hydrologic cycle. *Nature*, *419*(6903), 228.

Arakawa, A., & Schubert, W. H. (1974). Interaction of a cumulus cloud ensemble with the Large-Scale environment, part I. *J. Atmos. Sci.*, *31*(3), 674–701.

Betts, A. K. (1998, May). Climate-Convection feedbacks: Some further issues. *Climatic Change; Dordrecht*, *39*(39), 35–38. doi: 10.1023/A:1005323805826

Betts, A. K., & Ridgway, W. (1989, September). Climatic equilibrium of the atmospheric convective boundary layer over a tropical ocean. *J. Atmos. Sci.*, *46*(17), 2621–2641. doi: 10.1175/1520-0469(1989)046⟨2621:CEOTAC⟩2.0.CO;2

Bui, H. X., & Maloney, E. D. (2018). Changes in Madden-Julian oscillation precipitation and wind variance under global warming. *Geophys. Res. Lett.*.

Bui, H. X., & Maloney, E. D. (2019, November). Transient response of MJO precipitation and circulation to greenhouse gas forcing. *Geophys. Res. Lett.*, *7*, 847. doi: 10.1029/2019GL085328

Burt, M. A. (2016). *Interactions of arctic clouds, radiation, and sea ice in present-day and future climates* (Unpublished doctoral dissertation). Colorado State University. Libraries.

Byrne, M. P., Pendergrass, A. G., Rapp, A. D., & Wodzicki, K. R. (2018, August). Response of the intertropical convergence zone to climate change: Location, width, and strength. *Curr Clim Change Rep*, *4*(4), 355–370. doi: 10.1007/s40641-018-0110-5

Ceppi, P., & Hartmann, D. L. (2016, January). Clouds and the atmospheric circulation response to warming. *J. Clim.*, *29*(2), 783–799. doi: 10.1175/JCLI-D-15-0394.1

Charney, J. G. (1963). A note on large-scale motions in the tropics. *Journal of the Atmospheric Sciences*, *20*(6), 607–609.

Chikira, M. (2014, February). Eastward-Propagating intraseasonal oscillation represented by Chikira–Sugiyama cumulus parameterization. part II: Understanding moisture variation under weak temperature gradient balance. *J. Atmos. Sci.*, *71*(2), 615–639. doi: 10.1175/JAS-D-13-038.1

Chou, C., & Chen, C.-A. (2010, June). Depth of convection and the weakening of tropical circulation in global warming. *J. Clim.*, *23*(11), 3019–3030. doi: 10.1175/2010JCLI3383.1

Chou, C., & Neelin, J. D. (2004, July). Mechanisms of global warming impacts on regional tropical precipitation. *J. Clim.*, *17*(13), 2688–2701. doi: 10.1175/1520-0442(2004)017⟨2688:MOGWIO⟩2.0.CO;2

Emanuel, K. (2019, January). Inferences from simple models of slow, convectively coupled processes. *J. Atmos. Sci.*, *76*(1), 195–208. doi: 10.1175/JAS-D-18-0090.1

Feldl, N., Frierson, D. M. W., & Roe, G. H. (2014, March). The influence of regional feedbacks on circulation sensitivity. *Geophys. Res. Lett.*, *41*(6), 2212–2220. doi: 10.1002/2014GL059336

Grabowski, W. W. (2001, May). Coupling cloud processes with the Large-Scale dynamics using the Cloud-Resolving convection parameterization (CRCP). *J. Atmos. Sci.*, *58*(9), 978–997. doi: 10.1175/1520-0469(2001)058⟨0978:CCPWTL⟩2.0.CO;2

Held, I. M., & Soden, B. J. (2006, November). Robust responses of the hydrological cycle to global warming. *J. Clim.*, *19*(21), 5686–5699. doi: 10.1175/JCLI3990.1

Houze, R. A., Jr. (1977). Structure and dynamics of a tropical squall–line system. *Monthly Weather Review*, *105*(12), 1540–1567.

Khairoutdinov, M., Randall, D., & DeMott, C. (2005, July). Simulations of the atmospheric general circulation using a Cloud-Resolving model as a superparameterization of physical processes. *J. Atmos. Sci.*, *62*(7), 2136–2154. doi: 10.1175/JAS3453.1

Khairoutdinov, M., & Randall, D. A. (2001, September). A cloud resolving model as a cloud parameterization in the NCAR community climate system model: Preliminary results. *Geophys. Res. Lett.*, *28*(18), 3617–3620. doi: 10.1029/2001GL013552

Knutson, T. R., & Manabe, S. (1995, September). Time-Mean response over the tropical pacific to increased C02 in a coupled Ocean-Atmosphere model. *J. Clim.*, *8*(9), 2181–2199. doi: 10.1175/1520-0442(1995)008⟨2181:TMROTT⟩2.0.CO;2

Lutsko, N. J., & Cronin, T. W. (2018, November). Increase in precipitation efficiency with surface warming in RadiativeConvective equilibrium. *J. Adv. Model. Earth Syst.*, *10*(11), 2992–3010. doi: 10.1029/2018MS001482

Ma, J., & Xie, S.-P. (2013, April). Regional patterns of sea surface temperature change: A source of uncertainty in future projections of precipitation and atmospheric circulation. *J. Clim.*, *26*(8), 2482–2501. doi: 10.1175/JCLI-D-12-00283.1

Maher, P., Vallis, G. K., Sherwood, S. C., Webb, M. J., & Sansom, P. G. (2018, April). The impact of parameterized convection on climatological precipitation in atmospheric global climate models. *Geophys. Res. Lett.*, *45*(8), 3728–3736. doi: 10.1002/2017GL076826

Merlis, T. M. (2015, October). Direct weakening of tropical circulations from masked CO2 radiative forcing. *Proc. Natl. Acad. Sci. U. S. A.*, *112*(43), 13167–13171. doi: 10.1073/pnas.1508268112

Muller, C. J., O'Gorman, P. A., & Back, L. E. (2011, June). Intensification of precipitation extremes with warming in a Cloud-Resolving model. *J. Clim.*, *24*(11), 2784–2800. doi: 10.1175/2011JCLI3876.1

Randall, D., DeMott, C., Stan, C., Khairoutdinov, M., Benedict, J., McCrary, R., ... Branson, M. (2016, April). Simulations of the tropical general circulation with a multiscale global model. *Meteorol. Monogr.*, *56*, 15.1–15.15. doi: 10.1175/AMSMONOGRAPHS-D-15-0016.1

Randall, D., Khairoutdinov, M., Arakawa, A., & Grabowski, W. (2003). Breaking the cloud parameterization deadlock. *Bull. Am. Meteorol. Soc.*, *84*(11), 1547–1564. doi: 10.1175/BAMS-84-11-1547

Riehl, H., & Malkus, J. (1958). On the heat balance of the equatorial trough zone. geophysica. *Helsinki*, *6*, 3–4.

Schneider, T., O'Gorman, P. A., & Levine, X. J. (2010, July). WATER VAPOR AND THE DYNAMICS OF CLIMATE CHANGES. *Rev. Geophys.*, *48*(3), D22104. doi: 10.1029/2009RG000302

Seager, R., Naik, N., & Vecchi, G. A. (2010, September). Thermodynamic and dynamic mechanisms for Large-Scale changes in the hydrological cycle in response to global warming. *J. Clim.*, *23*(17), 4651–4668. doi: 10.1175/2010JCLI3655.1

Singh, M. S., & O'Gorman, P. A. (2015, October). Increases in moist-convective updraught velocities with warming in radiative-convective equilibrium: Increases in updraught velocities with warming. *Q.J.R. Meteorol. Soc.*, *141*(692), 2828–2838. doi: 10.1002/qj.2567

Sobel, A. H., & Bretherton, C. S. (2000, December). Modeling tropical precipitation in a single column. *J. Clim.*, *13*(24), 4378–4392. doi: 10.1175/1520-0442(2000)013⟨4378:MTPIAS⟩2.0.CO;2

Sobel, A. H., Nilsson, J., & Polvani, L. M. (2001, December). The weak temperature gradient approximation and balanced tropical moisture waves. *J. Atmos. Sci.*, *58*(23), 3650–3665. doi: 10.1175/1520-0469(2001)058⟨3650:TWTGAA⟩2.0.CO;2

Stevens, B., Satoh, M., Auger, L., Biercamp, J., Bretherton, C. S., Chen, X., ... others (2019). Dyamond: the dynamics of the atmospheric general circulation modeled on non-hydrostatic domains. *Progress in Earth and Planetary Science*, *6*(1), 61.

Su, H., Jiang, J. H., Zhai, C., Shen, T. J., Neelin, J. D., Stephens, G. L., & Yung, Y. L. (2014). Weakening and strengthening structures in the hadley circulation change under global warming and implications for cloud response and climate sensitivity. *J. Geophys. Res. D: Atmos.*, *119*(10), 5787–5805.

Vecchi, G. A., & Soden, B. J. (2007, September). Global warming and the weakening of the tropical circulation. *J. Clim.*, *20*(17), 4316–4340. doi: 10.1175/JCLI4258.1

Voigt, A., & Shaw, T. A. (2015, January). Circulation response to warming shaped by radiative changes of clouds and water vapour. *Nat. Geosci.*, *8*, 102. doi: 10.1038/ngeo2345

Wing, A. A., Reed, K. A., Satoh, M., Stevens, B., Bony, S., & Ohno, T. (2018, March). Radiative–convective equilibrium model intercomparison project. *Geoscientific Model Development*, *11*(2), 793–813. doi: 10.5194/gmd-11-793-2018

Wolding, B. O., Maloney, E. D., Henderson, S., & Branson, M. (2017, March). Climate change and the Madden-Julian oscillation: A vertically resolved weak temperature gradient analysis: CLIMATE CHANGE AND THE MJO. *Journal of Advances in Modeling Earth Systems*, *9*(1), 307–331. doi: 10.1002/2016MS000843